

MT Forward Modeling of 3-D Anisotropic Electrical Conductivity Structures Using the Rayleigh-Fourier Method

Patricia MARTINELLI* and Ana OSELLA*

Dto. de Física, Fac. Cs. Exactas y Naturales, Universidad de Buenos Aires, Ciudad Universitaria, Pab.1, 1428, Buenos Aires, Argentina

(Received October 30, 1996; Revised April 30, 1997; Accepted May 28, 1997)

We present an algorithm for modeling the magnetotelluric response of three-dimensional multilayered structures with irregular interfaces. In this formulation, based on a Rayleigh-Fourier technique, the effect of vertical anisotropy in the electrical conductivity has also been included. This method has an applicability range complementary to other solutions based on finite differences or on integral equations, which are especially adequate to model localized bodies intruded in a host medium.

To test the method, the MT response of a simple conductive structure was modeled and compared with the solutions obtained using integral equations. A good agreement between the results with similar processing times have been observed. Finally, the effect of anisotropy was estimated for the particular case of a conductive basin, showing a non-negligible contribution, depending on the relation between the vertical and horizontal values of the conductivity.

1. Introduction

The magnetotelluric method has been proved to be the one of most reliable ways to characterize crustal and upper mantle regional conductivity anomalies. The interpretation of MT data requires the application of numerical methods to model the geoelectrical structures. Due to the complexity of them, they are often simplified assuming a 2-D geometry.

Several methods have been developed for 2-D modeling, usually using finite element and finite difference techniques (e.g., Wannamaker *et al.*, 1987; Smith and Booker, 1991) or Rayleigh-Fourier expansions (e.g., Jiracek *et al.*, 1989; Osella and Martinelli, 1993). In order to determine the applicability of these models for the interpretation of field data, a previous analysis of distortions have to be performed. Different diagnostic tests have been developed to establish the dimension of the structure and the best way to approach it (Bahr, 1988; Groom and Bailey, 1989). Though for many studies, the 2-D modeling can give a realistic interpretation of data, the presence of 3-D structures introduces strong distortions to the electromagnetic responses (see e.g., Livelybrooks *et al.*, 1996; Mackie *et al.*, 1996; Pomposiello *et al.*, 1996).

In recent years, many efforts have been focused to solve this kind of problems. First methods have been developed using integral equation (IE) approaches (e.g., Hohmann, 1975; Wannamaker, 1991). These methods are specially adequate when dealing with a few number of blocks embedded in a 1-D layered medium, but become difficult to apply when the complexity of the structure increases.

3-D modeling using difference equations (DE) have been carried out, e.g., by Mackie *et al.* (1993) and Livelybrooks (1993). In these papers, 3-D algorithms were proposed which let to model more arbitrary complex media, using finite differences on a staggered grid. The design of the grid becomes then an important element in the description of the model, and again the

*Also at CONICET (Consejo Nacional de Investigaciones Científicas y Técnicas).

complexity increases as the structure is more variable, specially when changes occur in a gradual way.

In a previous paper, we have developed an algorithm to model the MT response of 2-D structures composed of homogeneous anisotropic layers with smooth irregular boundaries, using a Rayleigh-Fourier (RF) technique. Results obtained with this method were in agreement with the ones obtained by finite elements and finite differences for some simple structures and have proved to be more adequate when large scale variations are involved (e.g., Osella *et al.*, 1993). Then, in the present paper, we modify this method in order to apply it to model 3-D structures. The development of this method is performed assuming anisotropic media. We apply it to a conductive intrusion model and compare the results with the ones obtained using integral equations, from Wannamaker (1991) and also with the curves obtained assuming a 2-D behavior. Finally, we model a conductive basin to evaluate the effect produced by vertical electric anisotropy.

2. Theoretical Model

The method is formulated for 3-D layered structures with irregular boundaries described by functions $z = S_n(x, y)$ with $1 \leq n \leq N - 1$ (see Fig. 1).

It is assumed that each medium is linear, homogeneous and non-magnetic, but the model includes the possibility of vertical anisotropy of the electrical conductivity; the electric and magnetic field vectors have a harmonic time dependence $\exp(i\omega t)$. For the frequencies ω employed in magnetotelluric soundings and for the conductivities usually encountered, the quasi-stationary approximation is valid; then inside the earth, in layer n , the fields satisfy:

$$\nabla \times \bar{E}_n = -i\omega\mu_0 \bar{H}_n, \tag{1}$$

$$\nabla \times \bar{H}_n = \sigma_n \bar{E}_n \tag{2}$$

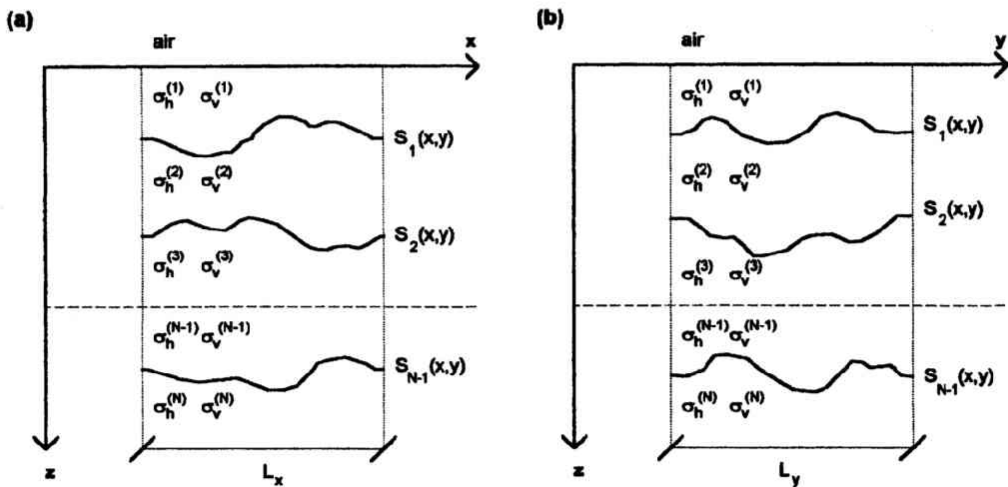


Fig. 1. Proposed N -layered model. Interfaces are functions of x and y . The electrical conductivity of each medium can present electrical anisotropy.

where μ_0 is the magnetic permeability of free space and

$$\sigma_n = \begin{pmatrix} \sigma_h^{(n)} & 0 & 0 \\ 0 & \sigma_h^{(n)} & 0 \\ 0 & 0 & \sigma_v^{(n)} \end{pmatrix} \quad (3)$$

the electrical conductivity tensor.

In the air (medium 0):

$$\nabla^2 \bar{H}_0 = 0. \quad (4)$$

The unknown external field, that can be considered horizontal and spatially uniform, has the form:

$$\bar{H}_e(\omega) = \left(H_x^{(e)}(\omega) \hat{x} + H_y^{(e)}(\omega) \hat{y} \right). \quad (5)$$

Then, defining $\bar{H}_{hor,n}$ and $\bar{E}_{hor,n}$ as:

$$\bar{H}_{hor,n}(x, y, z, \omega) = H_x^{(n)}(x, y, z, \omega) \hat{x} + H_y^{(n)}(x, y, z, \omega) \hat{y}, \quad (6)$$

$$\bar{E}_{hor,n}(x, y, z, \omega) = E_x^{(n)}(x, y, z, \omega) \hat{x} + E_y^{(n)}(x, y, z, \omega) \hat{y}, \quad (7)$$

and taking into account the linearity of Maxwell equations, the following relations can be written:

$$\bar{H}_{hor,n}(x, y, z, \omega) = \eta_n(x, y, z, \omega) \bar{H}_e(\omega), \quad (8)$$

$$H_z^{(n)}(x, y, z, \omega) = \bar{\eta}_{z,n}(x, y, z, \omega) \bar{H}_e(\omega), \quad (9)$$

$$\bar{E}_{hor,n}(x, y, z, \omega) = \xi_n(x, y, z, \omega) \bar{H}_e(\omega), \quad (10)$$

$$E_z^{(n)}(x, y, z, \omega) = \bar{\xi}_{z,n}(x, y, z, \omega) \bar{H}_e(\omega) \quad (11)$$

where the quantities η_n and ξ_n , which are tensors of dimension (2×2) , and $\bar{\eta}_{z,n}$ and $\bar{\xi}_{z,n}$, which are file vectors of dimension 2, do not depend on the inducing field. Then, the impedance tensor, \mathbf{Z} , and the tipper, \bar{T} , are given by:

$$\mathbf{Z}(x, y, \omega) = \xi_1(x, y, 0, \omega) \eta_1^{-1}(x, y, 0, \omega), \quad (12)$$

$$\bar{T}(x, y, \omega) = \bar{\eta}_{z,1}(x, y, 0, \omega) \eta_1^{-1}(x, y, 0, \omega). \quad (13)$$

They are calculated obtaining the response at the earth surface for two different linearly polarized external fields, one in the x direction and the other in the y direction. This is done applying Rayleigh's scattering theory on every interface. As it is well known, as some multiple reflections are not included in Rayleigh's formalism, it actually constitutes an approximation. However, this approximation works well in many cases provided that boundary slopes are not too large (Lippmann, 1953; Miller, 1971); using the method presented here, structures have been accurately modeled having maximum boundary slopes between 50 and 60 degrees, depending on layer resistivities.

The treatment can be simplified assuming that the interfaces $S_n(x, y)$ are even and periodic functions of x and y , their periodicities namely λ_x and λ_y . The studied area (see Fig. 1) corresponds to points (x, y) such that $|x - \lambda_x/4| \leq L_x/2$ and $|y - \lambda_y/4| \leq L_y/2$; outside this zone, that is, for points such that $L_x/2 < |x - \lambda_x/4| \leq \lambda_x/2$ and $L_y/2 < |y - \lambda_y/4| \leq \lambda_y/2$, the interfaces are plane. The effect that the imposed symmetries and periodicities exert over the zone of interest can be neglected if λ_x and λ_y are taken long as compared with L_x and L_y .

2.1 External field polarized in the x direction

When \overline{H}_e has the form:

$$\overline{H}_e(\omega) = H_x^{(e)}(\omega)\hat{x} \quad (14)$$

from Eq. (5) and Eqs. (8) to (11) it is obtained that:

$$H_j^{(n)}(x, y, z, \omega) = \eta_{jx}^{(n)}(x, y, z, \omega)H_x^{(e)}(\omega), \quad (15)$$

$$E_j^{(n)}(x, y, z, \omega) = \xi_{jx}^{(n)}(x, y, z, \omega)H_x^{(e)}(\omega) \quad (16)$$

with $j = x, y$ and z .

Due to the imposed symmetries and periodicity, $\eta_{jx}^{(n)}$ and $\xi_{jx}^{(n)}$ can be written as:

$$\eta_{xx}^{(n)}(x, y, z, \omega) = \sum_{l,m \geq 0} f_{l,m}^{(n)}(z, \omega) \cos(k_{xl}x) \cos(k_{ym}y), \quad (17)$$

$$\eta_{yx}^{(n)}(x, y, z, \omega) = - \sum_{l,m \geq 0} g_{l,m}^{(n)}(z, \omega) \sin(k_{xl}x) \sin(k_{ym}y), \quad (18)$$

$$\eta_{zx}^{(n)}(x, y, z, \omega) = \sum_{l,m \geq 0} h_{l,m}^{(n)}(z, \omega) \sin(k_{xl}x) \cos(k_{ym}y), \quad (19)$$

$$\xi_{xx}^{(n)}(x, y, z, \omega) = - \sum_{l,m \geq 0} p_{l,m}^{(n)}(z, \omega) \sin(k_{xl}x) \sin(k_{ym}y), \quad (20)$$

$$\xi_{yx}^{(n)}(x, y, z, \omega) = \sum_{l,m \geq 0} q_{l,m}^{(n)}(z, \omega) \cos(k_{xl}x) \cos(k_{ym}y), \quad (21)$$

$$\xi_{zx}^{(n)}(x, y, z, \omega) = - \sum_{l,m \geq 0} r_{l,m}^{(n)}(z, \omega) \cos(k_{xl}x) \sin(k_{ym}y) \quad (22)$$

with:

$$k_{xl} = 2l\pi/\lambda_x, \quad (23)$$

$$k_{ym} = 2m\pi/\lambda_y. \quad (24)$$

For $n \geq 1$, replacing Eq. (2) in Eq. (1) and defining:

$$\gamma_n^2 = i\omega\mu_0\sigma_h^{(n)}, \quad (25)$$

$$\alpha_n = \frac{\sigma_h^{(n)}}{\sigma_v^{(n)}}, \quad (26)$$

the following is obtained:

$$(-\alpha_n \partial_y^2 - \partial_z^2 + \gamma_n^2)H_x^{(n)} + \alpha_n \partial_x \partial_y H_y^{(n)} + \partial_x \partial_z H_z^{(n)} = 0, \quad (27)$$

$$\alpha_n \partial_x \partial_y H_x^{(n)} + (-\alpha_n \partial_x^2 - \partial_z^2 + \gamma_n^2)H_y^{(n)} + \partial_y \partial_z H_z^{(n)} = 0, \quad (28)$$

$$\partial_x \partial_z H_x^{(n)} + \partial_y \partial_z H_y^{(n)} + (-\partial_x^2 - \partial_y^2 + \gamma_n^2)H_z^{(n)} = 0. \quad (29)$$

Parameters α_n measure layer anisotropies; they are usually greater or equal than one.

Considering Eqs. (15), (17), (18) and (19), it is found that $\forall l, m \geq 0$ the functions $f_{lm}^{(n)}$, $g_{lm}^{(n)}$ and $h_{lm}^{(n)}$ satisfy the equations:

$$(\alpha_n k_{ym}^2 + \gamma_n^2)f_{lm}^{(n)} - \frac{d^2 f_{lm}^{(n)}}{dz^2} - \alpha_n k_{xl} k_{ym} g_{lm}^{(n)} + k_{xl} \frac{dh_{lm}^{(n)}}{dz} = 0, \quad (30)$$

$$-\alpha_n k_{xl} k_{ym} f_{lm}^{(n)} + (\alpha_n k_{xl}^2 + \gamma_n^2) g_{lm}^{(n)} - \frac{d^2 g_{lm}^{(n)}}{dz^2} + k_{ym} \frac{dh_{lm}^{(n)}}{dz} = 0, \quad (31)$$

$$-k_{xl} \frac{df_{lm}^{(n)}}{dz} - k_{ym} \frac{dg_{lm}^{(n)}}{dz} + (k_{xl}^2 + k_{ym}^2 + \gamma_n^2) h_{lm}^{(n)} = 0, \quad (32)$$

whose general solutions are (see Appendix):

$$\begin{aligned} f_{lm}^{(n)}(z, \omega) = & (\lambda k_{xl} + \delta_{l0} \delta_{m0}) (A_{lm}^{(n)}(\omega) \exp(R_{lm}^{(n)}(\omega)z) + B_{lm}^{(n)}(\omega) \exp(-R_{lm}^{(n)}(\omega)z)) \\ & + (\lambda k_{ym} + \delta_{l0} \delta_{m0}) (C_{lm}^{(n)}(\omega) \exp(Q_{lm}^{(n)}(\omega)z) \\ & + D_{lm}^{(n)}(\omega) \exp(-Q_{lm}^{(n)}(\omega)z)), \end{aligned} \quad (33)$$

$$\begin{aligned} g_{lm}^{(n)}(z, \omega) = & (\lambda k_{ym} + \delta_{l0} \delta_{m0}) (A_{lm}^{(n)}(\omega) \exp(R_{lm}^{(n)}(\omega)z) + B_{lm}^{(n)}(\omega) \exp(-R_{lm}^{(n)}(\omega)z)) \\ & - (\lambda k_{xl} + \delta_{l0} \delta_{m0}) (C_{lm}^{(n)}(\omega) \exp(Q_{lm}^{(n)}(\omega)z) \\ & + D_{lm}^{(n)}(\omega) \exp(-Q_{lm}^{(n)}(\omega)z)), \end{aligned} \quad (34)$$

$$h_{lm}^{(n)}(z, \omega) = \frac{\lambda k_{rlm}^2}{R_{lm}^{(n)}(\omega)} (A_{lm}^{(n)}(\omega) \exp(R_{lm}^{(n)}(\omega)z) - B_{lm}^{(n)}(\omega) \exp(-R_{lm}^{(n)}(\omega)z)) \quad (35)$$

where $\lambda = \sqrt{\lambda_x \lambda_y}$ and:

$$k_{rlm}^2 = k_{xl}^2 + k_{ym}^2, \quad (36)$$

$$(R_{lm}^{(n)})^2 = k_{rlm}^2 + \gamma_n^2, \quad (37)$$

$$(Q_{lm}^{(n)})^2 = \alpha_n k_{rlm}^2 + \gamma_n^2. \quad (38)$$

For each frequency, $A_{lm}^{(n)}$, $B_{lm}^{(n)}$, $C_{lm}^{(n)}$ and $D_{lm}^{(n)}$ are complex numbers that depend only on the subsurface structure. $B_{lm}^{(n)}$ and $D_{lm}^{(n)}$ are related with the upgoing fields and $A_{lm}^{(n)}$ and $C_{lm}^{(n)}$ with the downgoing ones.

Considering, from Eqs. (18) and (19), that $g_{lm}^{(n)}$ is undefined when l or m are 0 and $h_{0m}^{(n)}$ is undefined for any m , the value of these functions is chosen to be 0. To satisfy this condition it is necessary that:

$$A_{00}^{(n)} = C_{00}^{(n)}, \quad (39)$$

$$B_{00}^{(n)} = D_{00}^{(n)}, \quad (40)$$

$$A_{0m}^{(n)} = B_{0m}^{(n)} = C_{l0}^{(n)} = D_{l0}^{(n)} = 0. \quad (41)$$

Once the general solutions for the magnetic field have been found, the electric field can be obtained from Eq. (2). Considering Eqs. (20), (21) and (22), it results that:

$$\begin{aligned} p_{lm}^{(n)}(z, \omega) = & - \left(\frac{k_{ym}}{R_{lm}^{(n)}(\omega)} + \frac{\delta_{l0} \delta_{m0}}{\gamma_n(\omega) \lambda} \right) [A_{lm}^{(n)}(\omega) \exp(R_{lm}^{(n)}(\omega)z) - B_{lm}^{(n)}(\omega) \exp(-R_{lm}^{(n)}(\omega)z)] \\ & + \left(\frac{Q_{lm}^{(n)}(\omega) k_{xl}}{\gamma_n^2(\omega)} + \frac{\delta_{l0} \delta_{m0}}{\gamma_n(\omega) \lambda} \right) [C_{lm}^{(n)}(\omega) \exp(Q_{lm}^{(n)}(\omega)z) \\ & - D_{lm}^{(n)}(\omega) \exp(-Q_{lm}^{(n)}(\omega)z)], \end{aligned} \quad (42)$$

$$q_{lm}^{(n)}(z, \omega) = \left(\frac{k_{xl}}{R_{lm}^{(n)}(\omega)} + \frac{\delta_{l0} \delta_{m0}}{\gamma_n(\omega) \lambda} \right) [A_{lm}^{(n)}(\omega) \exp(R_{lm}^{(n)}(\omega)z) - B_{lm}^{(n)}(\omega) \exp(-R_{lm}^{(n)}(\omega)z)]$$

$$\begin{aligned}
 & + \left(\frac{Q_{lm}^{(n)}(\omega)k_{ym}}{\gamma_n^2(\omega)} + \frac{\delta_{l0}\delta_{m0}}{\gamma_n(\omega)\lambda} \right) [C_{lm}^{(n)}(\omega) \exp(Q_{lm}^{(n)}(\omega)z) \\
 & - D_{lm}^{(n)}(\omega) \exp(-Q_{lm}^{(n)}(\omega)z)], \tag{43}
 \end{aligned}$$

$$r_{lm}^{(n)}(z, \omega) = -\frac{\alpha_n}{\gamma_n^2(\omega)} k_{rlm}^2 [C_{lm}^{(n)}(\omega) \exp(Q_{lm}^{(n)}(\omega)z) + D_{lm}^{(n)}(\omega) \exp(-Q_{lm}^{(n)}(\omega)z)]. \tag{44}$$

In the air, taking into account that the external field is spatially uniform, the general solutions of Eq. (4) are:

$$f_{lm}^{(0)}(z, \omega) = (\lambda k_{xl} A_{lm}^{(0)}(\omega) + \lambda k_{ym} C_{lm}^{(0)}(\omega)) \exp(k_{rlm}z) + 2\delta_{l0}\delta_{m0}, \tag{45}$$

$$g_{lm}^{(0)}(z, \omega) = (\lambda k_{ym} A_{lm}^{(0)}(\omega) - \lambda k_{xl} C_{lm}^{(0)}(\omega)) \exp(k_{rlm}z), \tag{46}$$

$$h_{lm}^{(0)}(z, \omega) = \lambda k_{rlm} A_{lm}^{(0)}(\omega) \exp(k_{rlm}z) \tag{47}$$

with:

$$A_{0m}^{(0)} = C_{l0}^{(0)} = 0 \tag{48}$$

$\forall l, m \geq 0$.

When Rayleigh's approximations are valid the series (17) to (22) converge, so subscripts l and m can be truncated at a finite number L . This implies that the value of the fields inside each layer n in the earth is determined by $4L(L + 1) + 2$ coefficients, $A_{lm}^{(n)}$, $B_{lm}^{(n)}$, $C_{lm}^{(n)}$ and $D_{lm}^{(n)}$. Applying the adequate boundary conditions, the coefficients $A_{lm}^{(1)}$, $B_{lm}^{(1)}$, $C_{lm}^{(1)}$ and $D_{lm}^{(1)}$ that define the response at the earth surface can be calculated.

At the earth surface, H_x and H_y are continuous, then for each l and m greater or equal than 0, from Eqs. (33) to (35) and Eqs. (45) to (47), it is obtained that:

$$\begin{aligned}
 \lambda k_{xl} A_{lm}^{(0)}(\omega) + \lambda k_{ym} C_{lm}^{(0)}(\omega) + 2\delta_{l0}\delta_{m0} &= \lambda k_{xl} (A_{lm}^{(1)}(\omega) + B_{lm}^{(1)}(\omega)) + \lambda k_{ym} (C_{lm}^{(1)}(\omega) + D_{lm}^{(1)}(\omega)) \\
 &+ 2\delta_{l0}\delta_{m0} (A_{00}^{(1)}(\omega) + B_{00}^{(1)}(\omega)), \tag{49}
 \end{aligned}$$

$$\lambda k_{ym} A_{lm}^{(0)}(\omega) - \lambda k_{xl} C_{lm}^{(0)}(\omega) = \lambda k_{ym} (A_{lm}^{(1)}(\omega) + B_{lm}^{(1)}(\omega)) - \lambda k_{xl} (C_{lm}^{(1)}(\omega) + D_{lm}^{(1)}(\omega)). \tag{50}$$

On each interface n , with $1 \leq n \leq N - 1$, the tangential components of \vec{H} and \vec{E} are continuous. Then, considering Eq. (15) and Eqs. (17) to (19):

$$\begin{aligned}
 & \sum_{l,m \geq 0} f_{l,m}^{(n)}(S_n(x, y), \omega) \cos(k_{xl}x) \cos(k_{ym}y) \\
 & + \partial_x S_n(x, y) \sum_{l,m \geq 0} h_{l,m}^{(n)}(S_n(x, y), \omega) \sin(k_{xl}x) \cos(k_{ym}y) \\
 & = \sum_{l,m \geq 0} f_{l,m}^{(n+1)}(S_n(x, y), \omega) \cos(k_{xl}x) \cos(k_{ym}y) \\
 & + \partial_x S_n(x, y) \sum_{l,m \geq 0} h_{l,m}^{(n+1)}(S_n(x, y), \omega) \sin(k_{xl}x) \cos(k_{ym}y), \tag{51}
 \end{aligned}$$

$$\begin{aligned}
 & \sum_{l,m \geq 0} g_{l,m}^{(n)}(S_n(x, y), \omega) \sin(k_{xl}x) \sin(k_{ym}y) \\
 & - \partial_y S_n(x, y) \sum_{l,m \geq 0} h_{l,m}^{(n)}(S_n(x, y), \omega) \sin(k_{xl}x) \cos(k_{ym}y) \\
 & = \sum_{l,m \geq 0} g_{l,m}^{(n+1)}(S_n(x, y), \omega) \sin(k_{xl}x) \sin(k_{ym}y) \\
 & - \partial_y S_n(x, y) \sum_{l,m \geq 0} h_{l,m}^{(n+1)}(S_n(x, y), \omega) \sin(k_{xl}x) \cos(k_{ym}y) \tag{52}
 \end{aligned}$$

where $f_{l,m}^{(n)}$, $g_{l,m}^{(n)}$ and $h_{l,m}^{(n)}$ are given by Eqs. (33) to (35). On the same way, from Eq. (16) and Eqs. (20) to (22):

$$\begin{aligned} & \sum_{l,m \geq 0} p_{l,m}^{(n)}(S_n(x,y),\omega) \sin(k_{xl}x) \sin(k_{ym}y) \\ & \quad + \partial_x S_n(x,y) \sum_{l,m \geq 0} r_{l,m}^{(n)}(S_n(x,y),\omega) \cos(k_{xl}x) \sin(k_{ym}y) \\ & = \sum_{l,m \geq 0} p_{l,m}^{(n+1)}(S_n(x,y),\omega) \sin(k_{xl}x) \sin(k_{ym}y) \\ & \quad + \partial_x S_n(x,y) \sum_{l,m \geq 0} r_{l,m}^{(n+1)}(S_n(x,y),\omega) \cos(k_{xl}x) \sin(k_{ym}y), \end{aligned} \tag{53}$$

$$\begin{aligned} & \sum_{l,m \geq 0} q_{l,m}^{(n)}(S_n(x,y),\omega) \cos(k_{xl}x) \cos(k_{ym}y) \\ & \quad - \partial_y S_n(x,y) \sum_{l,m \geq 0} r_{l,m}^{(n)}(S_n(x,y),\omega) \cos(k_{xl}x) \sin(k_{ym}y) \\ & = \sum_{l,m \geq 0} q_{l,m}^{(n+1)}(S_n(x,y),\omega) \cos(k_{xl}x) \cos(k_{ym}y) \\ & \quad - \partial_y S_n(x,y) \sum_{l,m \geq 0} r_{l,m}^{(n+1)}(S_n(x,y),\omega) \cos(k_{xl}x) \sin(k_{ym}y) \end{aligned} \tag{54}$$

with $p_{l,m}^{(n)}$, $q_{l,m}^{(n)}$ and $r_{l,m}^{(n)}$ defined by Eqs. (42) to (44).

Multiplying Eq. (54) by $\cos(k_{xi}x) \cos(k_{yj}y)$, for $0 \leq i, j \leq L$, and Eq. (52) by $\sin(k_{xi}x) \sin(k_{yj}y)$, for $1 \leq i, j \leq L$, and then integrating over the rectangle $-\lambda_x/2 \leq x \leq \lambda_x/2$, $-\lambda_y/2 \leq y \leq \lambda_y/2$, $2L(L+1)+1$ linear equations that relate the coefficients A_{lm} , B_{lm} , C_{lm} and D_{lm} of the medium n with the ones of the medium $n+1$ are obtained. These equations do not depend on the coordinates. Giving a similar treatment to the Eqs. (53) and (54) which arise from the continuity of the tangential components of \vec{E} , $2L(L+1)+1$ additional relations are obtained. It must also be considered that in the deepest medium, N , $A_{lm}^{(N)}$ and $C_{lm}^{(N)}$ are 0.

These systems of equations are solved to obtain the functions η_{xx} , η_{yx} , η_{zx} , ξ_{xx} and ξ_{yx} for $n=1$, at $z=0$, using an analogous procedure to the one implemented for the 2-D case (Osella and Martinelli, 1993). This 2-D Rayleigh-Fourier method has been widely tested by comparison with FE and FD techniques to establish a self-consistency criterion for the determination of the validity of Rayleigh's approximation, in each particular case. As Rayleigh solutions are an approximation, there are residual discontinuities of the tangential components of the fields at layer interfaces. When the approximation is valid, the root mean squared values of these residuals can be reduced to a level below one or two points per cent; in addition, the series expansion of the field components converge. On the contrary, when the approximation is no more valid, the residual discontinuities are large, and cannot be reduced by increasing the number of scattering orders, L ; in these cases, either, the series directly exhibit an oscillatory behavior, or they are convergent for small values of L and then become divergent as L increases. These results are in agreement with those obtained by Jiracek *et al.* (1989), and they seem to be valid also for 3-D cases, as it has been observed analyzing the behavior of RF solutions of a great variety of 3-D structures. The maximum boundary slopes that can be correctly modeled lie typically in the range 50–60 degrees, but can exceed these values in very resistive cases.

2.2 External field polarized in the y direction

In this case \overline{H}_e is given by:

$$\overline{H}_e(\omega) = H_y^{(e)}(\omega)\widehat{y} \tag{55}$$

then, from Eq. (5) and Eqs. (8) to (11):

$$H_j^{(n)}(x, y, z, \omega) = \eta_{jy}^{(n)}(x, y, z, \omega)H_y^{(e)}(\omega), \tag{56}$$

$$E_j^{(n)}(x, y, z, \omega) = \xi_{jy}^{(n)}(x, y, z, \omega)H_y^{(e)}(\omega) \tag{57}$$

with $k = x, y$ and z .

Now, the existing symmetries imply that:

$$\eta_{xy}^{(n)}(x, y, z, \omega) = - \sum_{l,m \geq 0} f_{l,m}^{(n)}(z, \omega) \sin(k_{xl}x) \sin(k_{ym}y), \tag{58}$$

$$\eta_{yy}^{(n)}(x, y, z, \omega) = \sum_{l,m \geq 0} g_{l,m}^{(n)}(z, \omega) \cos(k_{xl}x) \cos(k_{ym}y), \tag{59}$$

$$\eta_{zy}^{(n)}(x, y, z, \omega) = - \sum_{l,m \geq 0} h_{l,m}^{(n)}(z, \omega) \cos(k_{xl}x) \sin(k_{ym}y), \tag{60}$$

$$\xi_{xy}^{(n)}(x, y, z, \omega) = \sum_{l,m \geq 0} p_{l,m}^{(n)}(z, \omega) \cos(k_{xl}x) \cos(k_{ym}y), \tag{61}$$

$$\xi_{yy}^{(n)}(x, y, z, \omega) = - \sum_{l,m \geq 0} q_{l,m}^{(n)}(z, \omega) \sin(k_{xl}x) \sin(k_{ym}y), \tag{62}$$

$$\xi_{zy}^{(n)}(x, y, z, \omega) = \sum_{l,m \geq 0} r_{l,m}^{(n)}(z, \omega) \sin(k_{xl}x) \cos(k_{ym}y). \tag{63}$$

For $n \geq 1$ it can be demonstrated that, for this polarization, the functions $f_{l,m}^{(n)}, g_{l,m}^{(n)}, h_{l,m}^{(n)}, p_{l,m}^{(n)}, q_{l,m}^{(n)}$ and $r_{l,m}^{(n)}$ also have the form shown in Eqs. (33) to (35) and Eqs. (42) to (44), but in this case:

$$A_{00}^{(n)} = -C_{00}^{(n)}, \tag{64}$$

$$B_{00}^{(n)} = -D_{00}^{(n)}, \tag{65}$$

$$A_{l0}^{(n)} = B_{l0}^{(n)} = C_{0m}^{(n)} = D_{0m}^{(n)} = 0. \tag{66}$$

In the medium 0, considering the form of the external field, it results:

$$f_{lm}^{(0)}(z, \omega) = (\lambda k_{xl}A_{lm}^{(0)}(\omega) + \lambda k_{ym}C_{lm}^{(0)}(\omega)) \exp(k_{rlm}z), \tag{67}$$

$$g_{lm}^{(0)}(z, \omega) = (\lambda k_{ym}A_{lm}^{(0)}(\omega) - \lambda k_{xl}C_{lm}^{(0)}(\omega)) \exp(k_{rlm}z) + 2\delta_{l0}\delta_{m0}, \tag{68}$$

$$h_{lm}^{(0)}(z, \omega) = \lambda k_{rlm}A_{lm}^{(0)}(\omega) \exp(k_{rlm}z) \tag{69}$$

with:

$$A_{l0}^{(0)} = C_{0m}^{(0)} = 0. \tag{70}$$

The response at the earth surface is obtained applying the same boundary conditions that in the last section, continuity of the tangential components of the fields on each interface $z = S_n(x, y)$, with $1 \leq n \leq N - 1$, and continuity of H_x and H_y at $z = 0$; then, the functions $\eta_{xy}, \eta_{yy}, \eta_{zy}, \xi_{xy}$ and ξ_{yy} , for $n = 1$ are obtained.

3. A Conductive Intrusion: Comparison of IE and RF Solutions and Evaluation of 3-D Effects

To test the formulation, its results are compared with those obtained using the IE method implemented by Wannamaker (1991), for an isotropic case.

The structure modeled by IE consists of a conductive cuboid embedded in a host, semi-infinite medium of resistivity 50 Ωm; the resistivity of the body ranges from 5 Ωm at its center to 30 Ωm at its border (Fig. 2(a)). This structure is approximated by a three layer, smooth model, with resistivities ρ₁ = 50 Ωm, ρ₂ = 5 Ωm and ρ₃ = 50 Ωm (Fig. 2(b)). The boundaries are described by the following function:

$$\text{if } 0 \leq x \leq x_0 \text{ and } 0 \leq y \leq y_0 : \quad S_n(x, y) = P + D_n, \tag{71}$$

$$\text{if } x_0 + G \leq x \text{ and } y_0 + G \leq y : \quad S_n(x, y) = P, \tag{72}$$

$$\text{if } x_0 \leq x \leq x_0 + G \text{ and } 0 \leq y \leq y_0 : \quad S_n(x, y) = P + \frac{D_n}{2} \left[1 + \cos \left(\frac{\pi(x - x_0)}{G} \right) \right], \tag{73}$$

if 0 ≤ x ≤ x₀ and y₀ ≤ y ≤ y₀ + G :

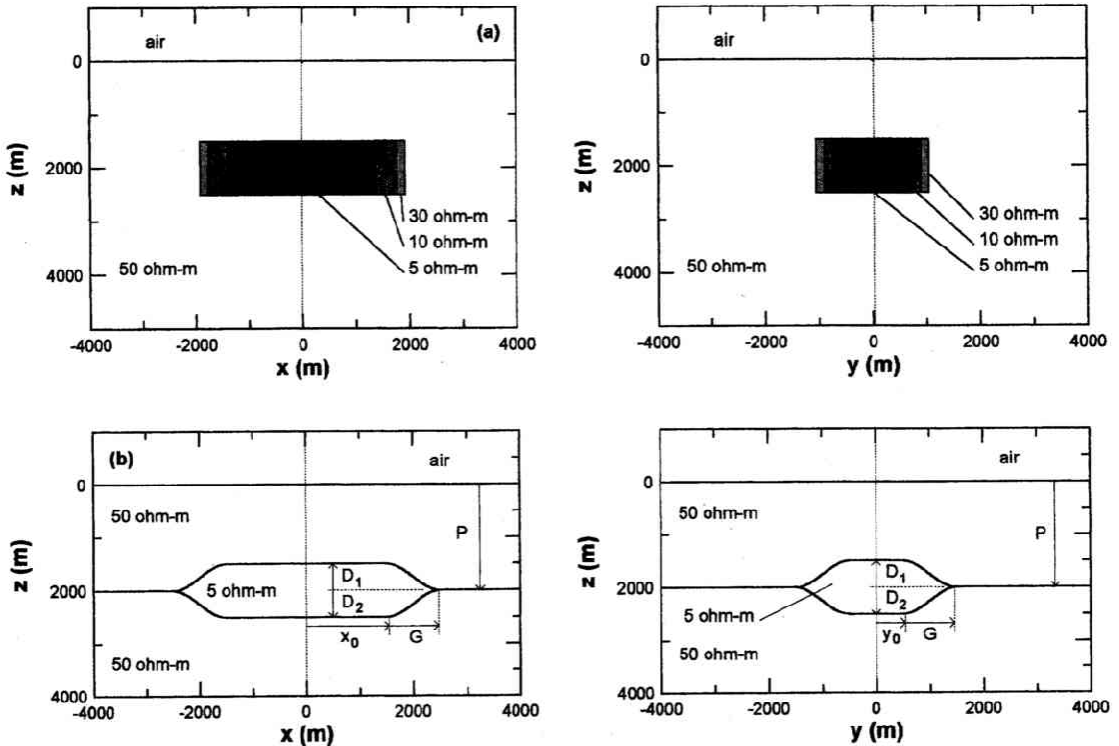


Fig. 2. Conductive intrusion models chosen to make the comparison between the IE method from Wannamaker (1991) (2a) and the RF method presented here (2b). Figure 2(b) also shows the geometrical meaning of the parameters involved in the definition of the interfaces (Eqs. (71) to (75)).

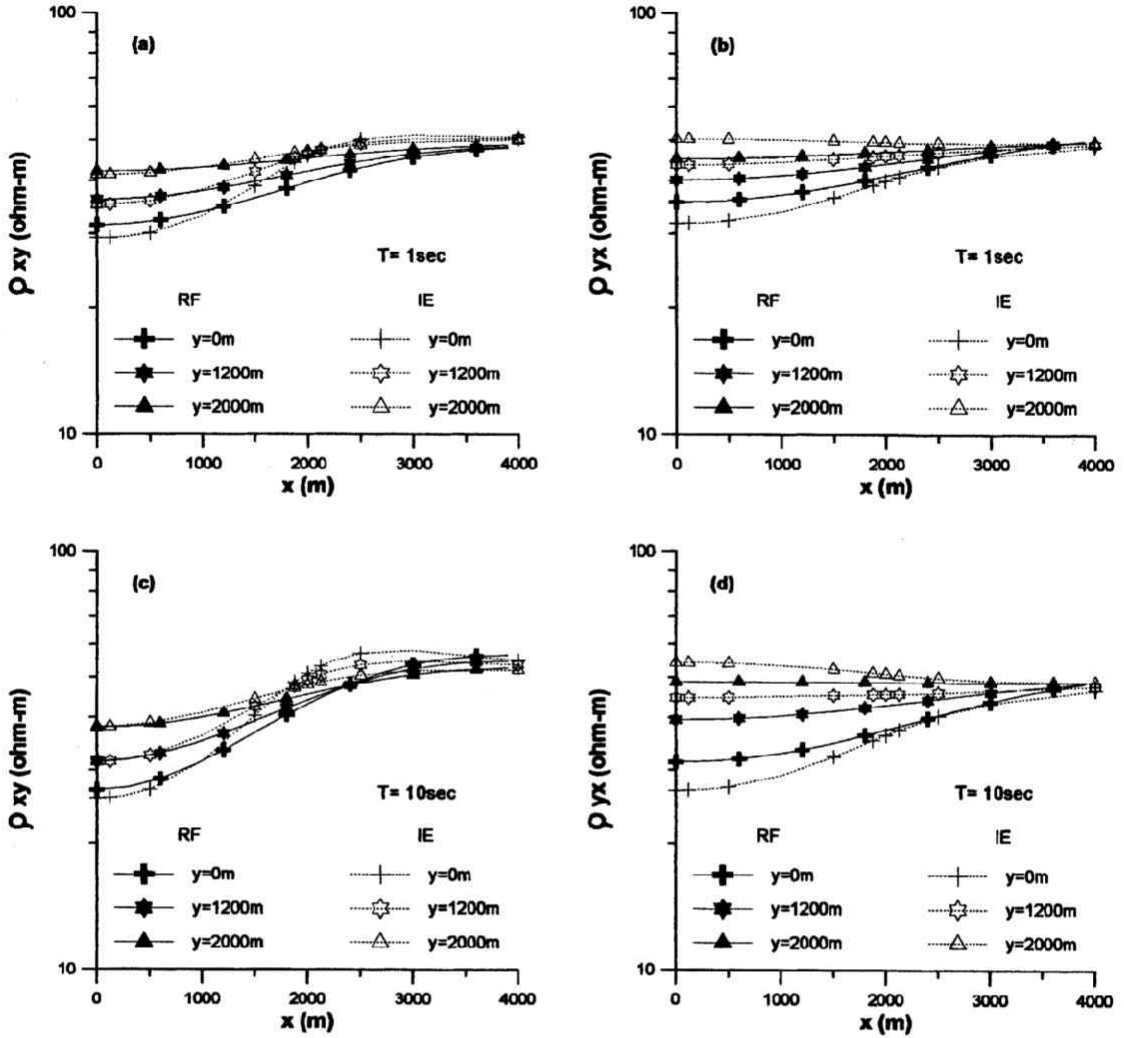


Fig. 3. Apparent resistivity curves ρ_{xy} and ρ_{yx} for the conducting cuboid obtained by IE together with the results corresponding to the smooth model calculated by RF.

$$S_n(x, y) = P + \frac{D_n}{2} \left[1 + \cos \left(\frac{\pi (y - y_0)}{G} \right) \right], \tag{74}$$

if $x_0 \leq x \leq x_0 + G$ and $y_0 \leq y \leq y_0 + G$:

$$S_n(x, y) = P + \frac{D_n}{4} \left[1 + \cos \left(\frac{\pi (x - x_0)}{G} \right) \right] \left[1 + \cos \left(\frac{\pi (y - y_0)}{G} \right) \right] \tag{75}$$

for $n = 1$ and 2 . Selected values of the parameters are: $x_0 = 1500$ m, $y_0 = 500$ m, $G = 1000$ m, $P = 2000$ m, $D_1 = -500$ m and $D_2 = 500$ m; their geometrical meaning is also indicated in Fig. 2(b).

Figures 3 and 4 show the response of the cuboid, obtained using IE, together with the results of the smooth model calculated by RF.

The dependence with x of the apparent resistivities ρ_{xy} and ρ_{yx} at different values of y can

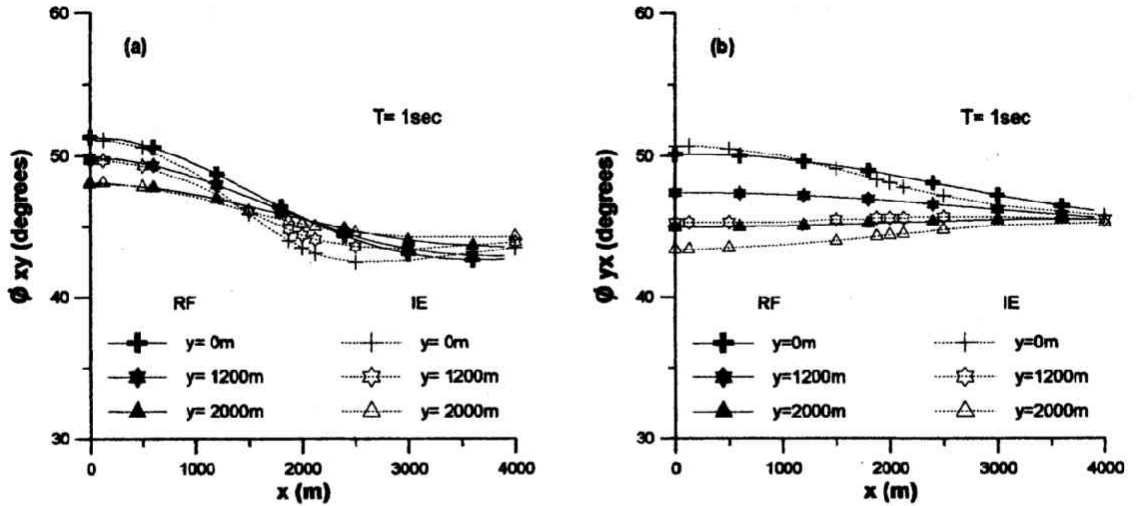


Fig. 4. The same as in Fig. 3 for the phases of the components of the impedance tensor ϕ_{xy} and ϕ_{yx} .

be seen in Figs. 3(a) and 3(b) for a period $T = 1$ sec, and in Figs. 3(c) and 3(d) for $T = 10$ sec; the phases of the components of the impedance tensor ϕ_{xy} and ϕ_{yx} , are shown only for $T = 1$ sec (Fig. 4) because the effect for $T = 10$ sec is negligible. Graphics are done only for positive values of x and y , considering that the curves are symmetric respect to the origin for the two coordinates.

The results obtained by each method are not coincident due to the differences between the models, but their general behavior is similar. Over the center of the structures, ρ_{xy} and ρ_{yx} reach their minimum values while ϕ_{xy} and ϕ_{yx} are maxima; for increasing x or y , apparent resistivities increase and phases decrease, and far from the intrusion they recover the values corresponding to the half space.

In particular, the values of ρ_{xy} for both models, which are related with the amount of current induced in the x direction, are quite similar in the central zone, and coincide outside the body. The greatest differences appear for x between 1500 m and 2500–3000 m; this can be attributed to the existence of border effects at the vertical contacts in the cuboid that tend to increase the apparent resistivity.

On the other hand, ρ_{yx} detects the differences between the structures for all the values of x and y over or near the anomaly, a result that can be understood taking into account that the body has less extension in the y direction.

The agreement found between the results obtained by each method is also better for ϕ_{xy} than for ϕ_{yx} .

The width in the y direction of the 3-D conducting body modeled by RF, whose interfaces are described by Eqs. (71) to (75), is determined by the value of the parameter y_0 . Making y_0 tend to infinite without changing the value of the other parameters, a 2-D structure with strike direction y that has the same x - z profile than the initial 3-D model, is obtained. Comparing the responses of these two models, the importance of three-dimensional effects can be analyzed.

The apparent resistivities of the 2-D and 3-D intrusions as functions of x at $y = 0$ are plotted in Fig. 5 and the phases are shown in Fig. 6. It must be noted that for this profile, in the 2-D case, the curves ρ_{xy} , ϕ_{xy} and ρ_{yx} , ϕ_{yx} correspond respectively, to the TM and TE modes. Two important conclusions are derived from these figures: the first is that the anomaly produced is greater in the 2-D case, the second is related with the behavior of ρ_{yx} and ϕ_{yx} curves. As it is well

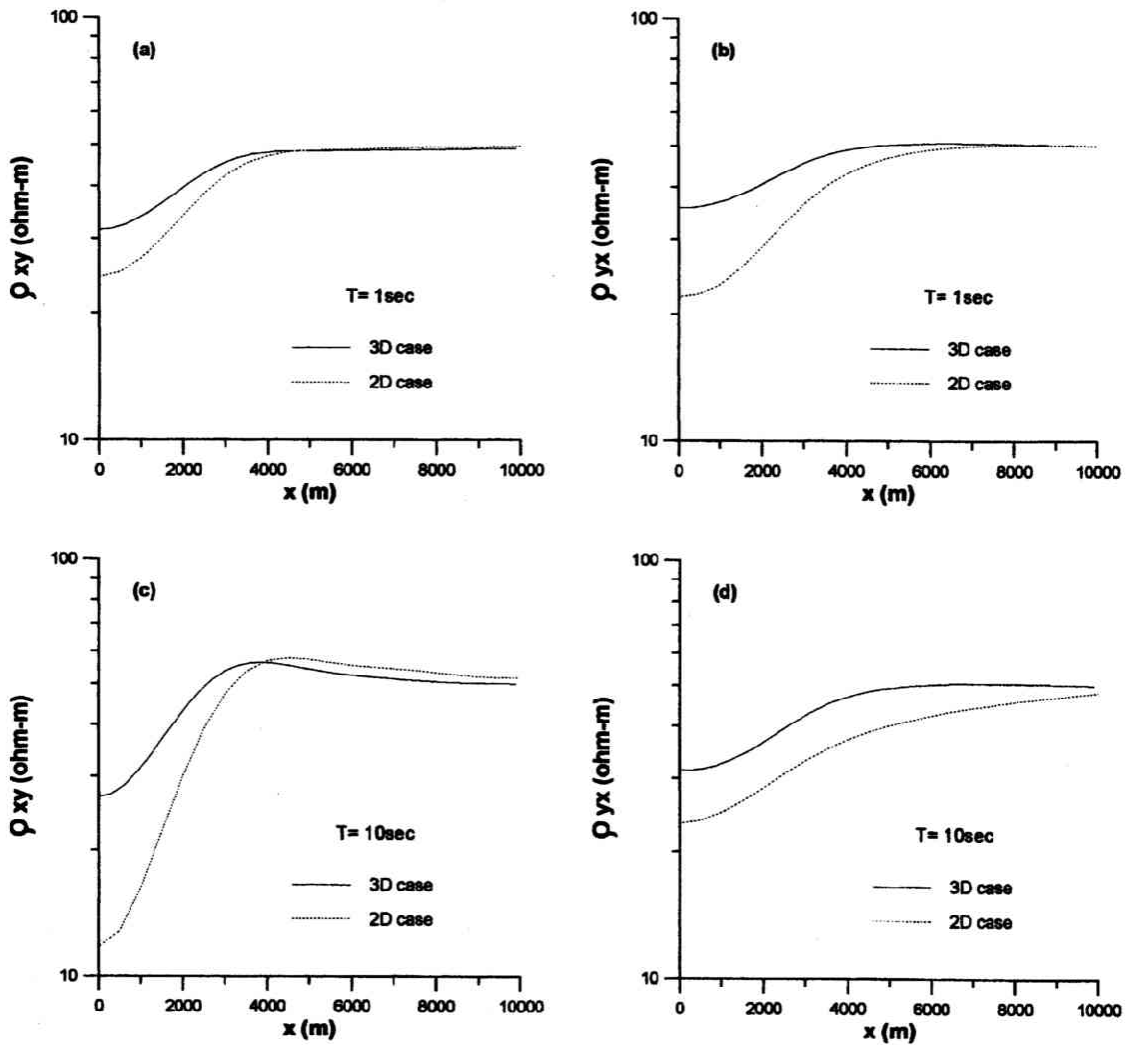


Fig. 5. Comparison between the apparent resistivity curves ρ_{xy} and ρ_{yx} , at $y = 0$, calculated by RF in the 3-D and 2-D cases.

known, for 2-D structures, the sensitivity of the TE response to the distribution of conductivity diminishes as the penetration depth of the fields increases. In the particular case presented here, TE resistivity and phase curves as functions of x , become progressively flatter than TM curves, as period increases. It can be seen from Figs. 5(c) and 5(d), that $\rho_{yx}(x)$ variations are clearly lower than $\rho_{xy}(x)$ variations, at $T = 10$ sec. On the other hand, a much lower effect is observed in the curves corresponding to the 3-D intrusion.

4. A Sedimentary Basin: Modeling and Evaluation of the Effect of Anisotropy

In this section, RF method is applied to model a 3-D basin. The structure proposed is composed of an upper sedimentary layer overlying a basement of resistivity $500 \Omega\text{m}$ (Fig. 7). The

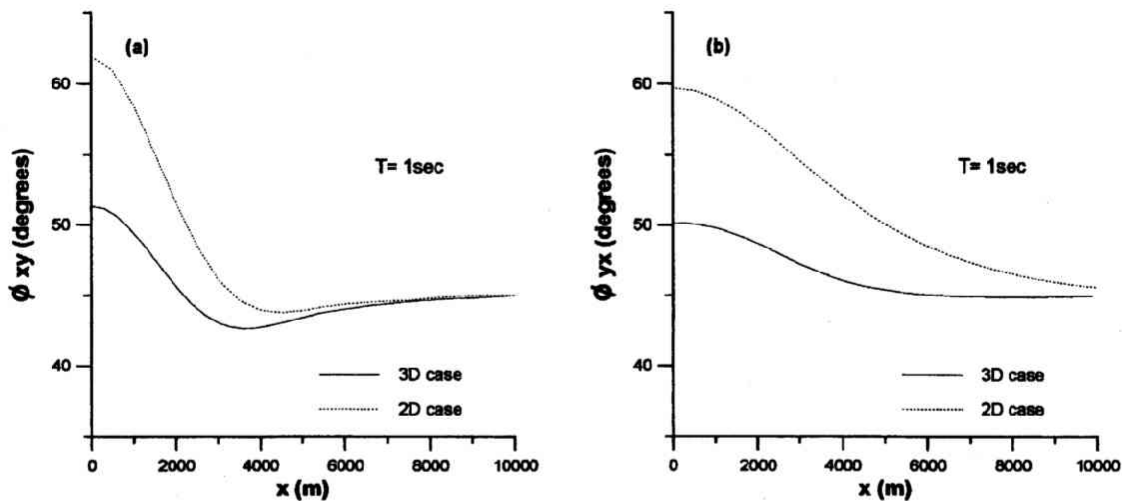


Fig. 6. Comparison between the phases ϕ_{xy} and ϕ_{yx} , at $y = 0$, calculated by RF in the 3-D and 2-D cases.

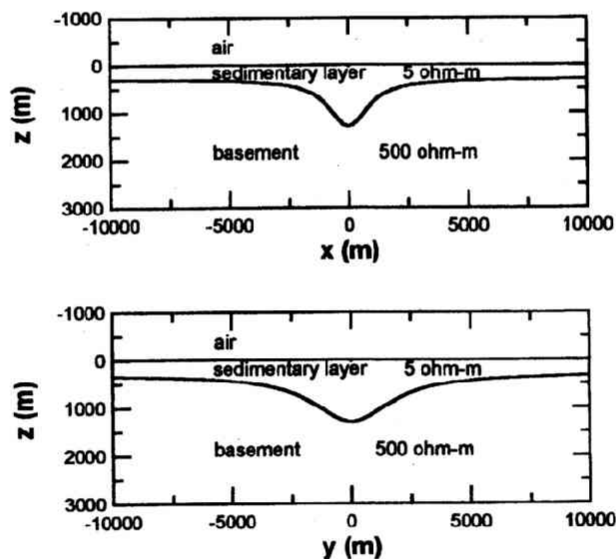


Fig. 7. Three-dimensional sedimentary basin model.

boundary between these layers is described by the following function:

$$S_n(x, y) = P + \frac{D}{\left[1 + \left(\frac{x}{G_x}\right)^2\right] \left[1 + \left(\frac{y}{G_y}\right)^2\right]} \tag{76}$$

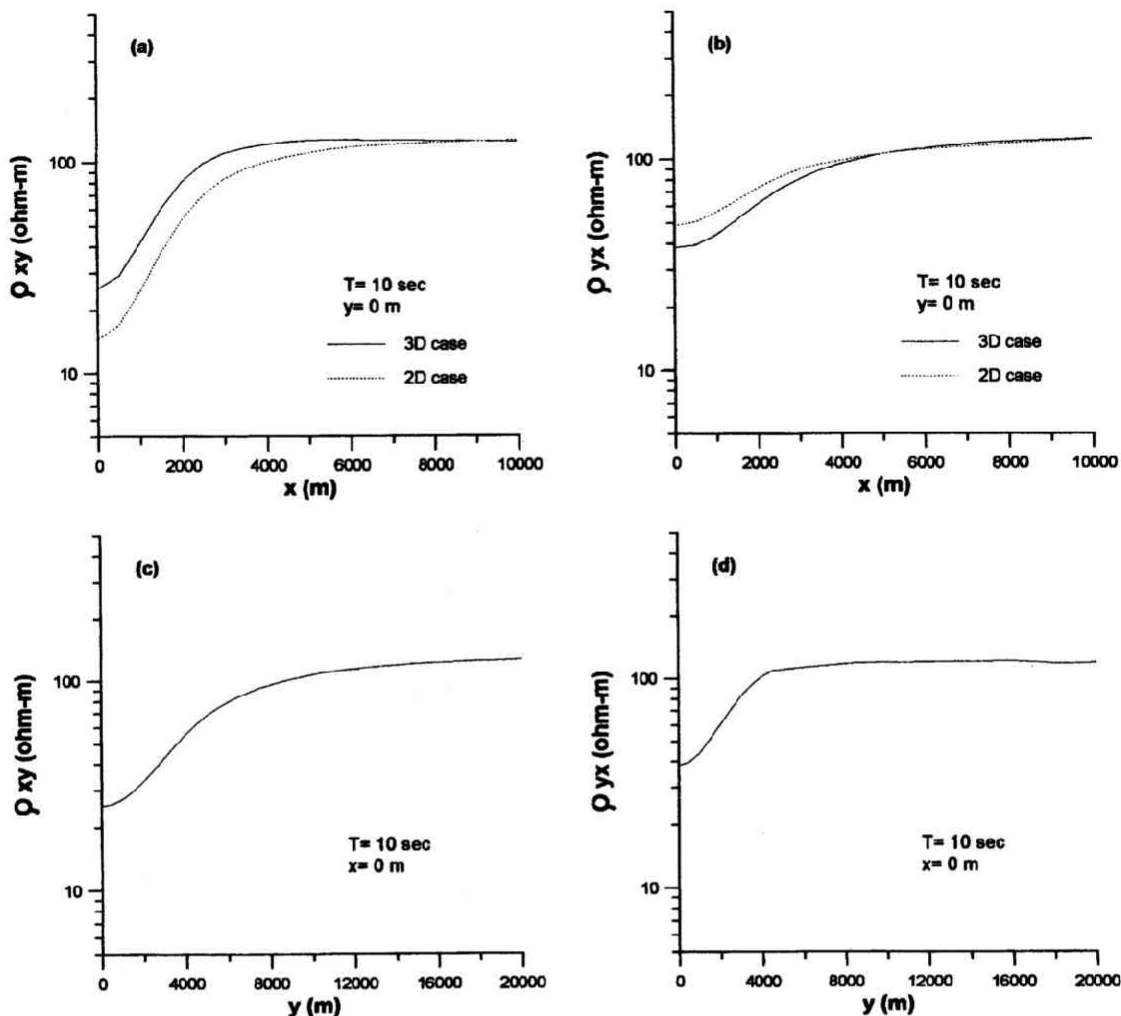


Fig. 8. Apparent resistivity curves ρ_{xy} and ρ_{yx} , obtained for the 3-D and 2-D models.

$P + D$ is the maximum sedimentary thickness, reached at $x = y = 0$; G_x and G_y are related to the lateral extension of the basin in the x and y directions, respectively. The selected values of the parameters were: $P = 300$ m, $D = 1000$ m, $G_x = 1000$ m and $G_y = 2000$ m; then, the extension of the basin is maximum in the y direction.

The first modeling was made assuming an isotropic sedimentary layer of resistivity $5 \Omega\text{m}$. The response of this structure, calculated at a representative period $T = 10$ sec for two perpendicular transects (one correspondent to set $y = 0$ and the other to set $x = 0$), is shown in Figs. 8 and 9. It is worth to be noted that this kind of structure would be difficult to model using the other methods.

Like in the case of the conductive intrusion, a decrease of the apparent resistivities occurs over the basin, but the anomaly is greater in this case.

In Figs. 8(a,b) and 9(a,b), the response of a 2-D structure with the same x - z profile than the 3-D basin, but with an infinite y extension, also is shown. In this case, ρ_{xy} and ϕ_{xy} give the TM

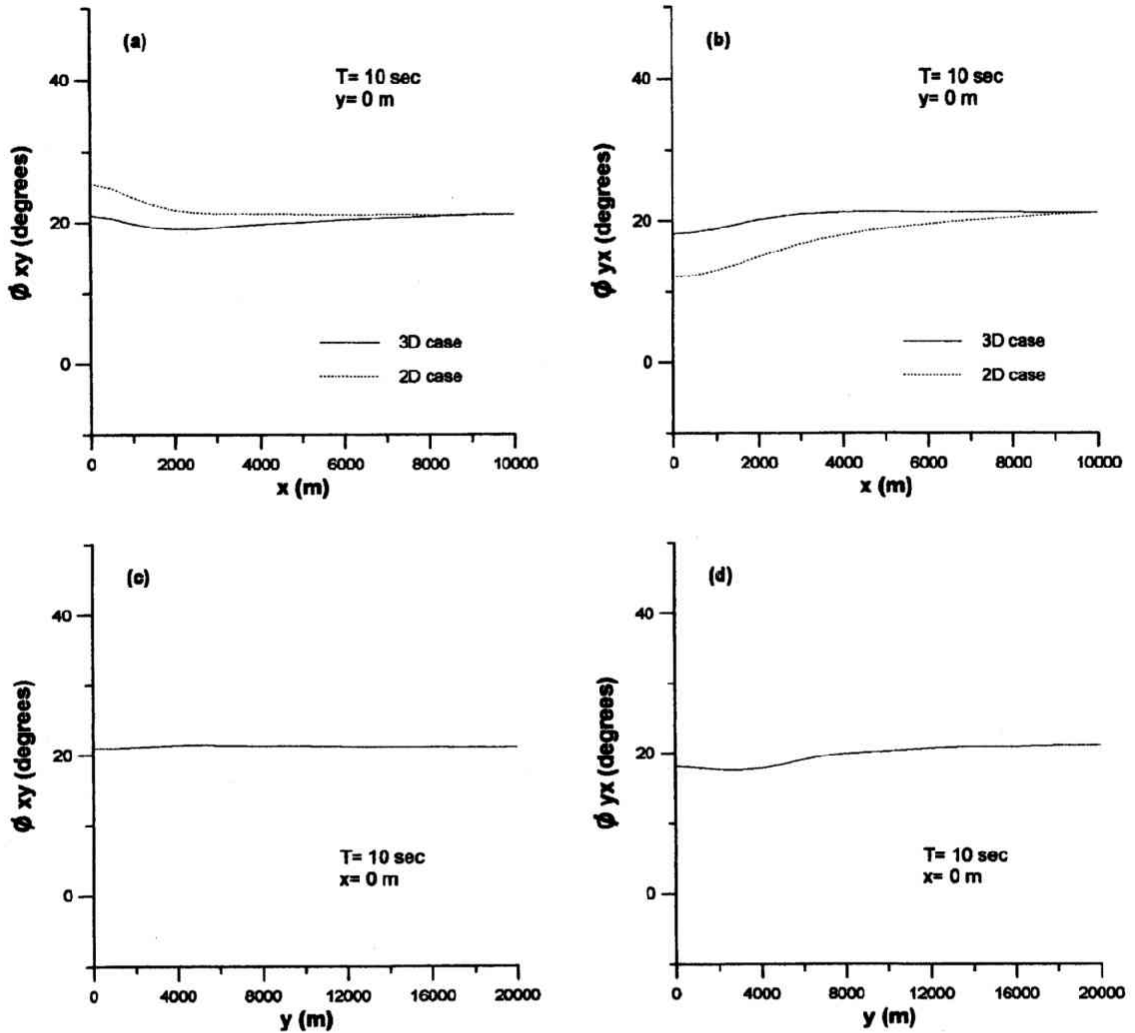


Fig. 9. The same as in Fig. 8 for the phases ϕ_{xy} and ϕ_{yx} .

response while ρ_{yx} and ϕ_{yx} correspond to the TE mode.

According to the discussion at the last section, for 2-D structures, at large periods, the TM response is more sensitive to the distribution of conductivity than the TE response; for example, at the center of the proposed 2-D basin, TE apparent resistivity is more than three times greater than TM resistivity. At the center of the 3-D basin, ρ_{yx} also is greater than ρ_{xy} , but in this case, the difference between these quantities is lower than in the 2-D case.

The same can be said about the values of ϕ_{xy} and ϕ_{yx} calculated over the center of each structure: the lowest difference is obtained for the 3-D model (see Figs. 9(a) and 9(b)).

It is shown next, how changes in the vertical resistivity of the sedimentary cover modify the response of the 3-D basin. The horizontal resistivity was not varied, but two different values were taken for the vertical resistivity: 25 Ωm and 1 Ωm ; the first corresponds to a factor of anisotropy (see Eq. (26)) $\alpha = 5$ and the second to $\alpha = 1/5$. As it was indicated previously, α is usually

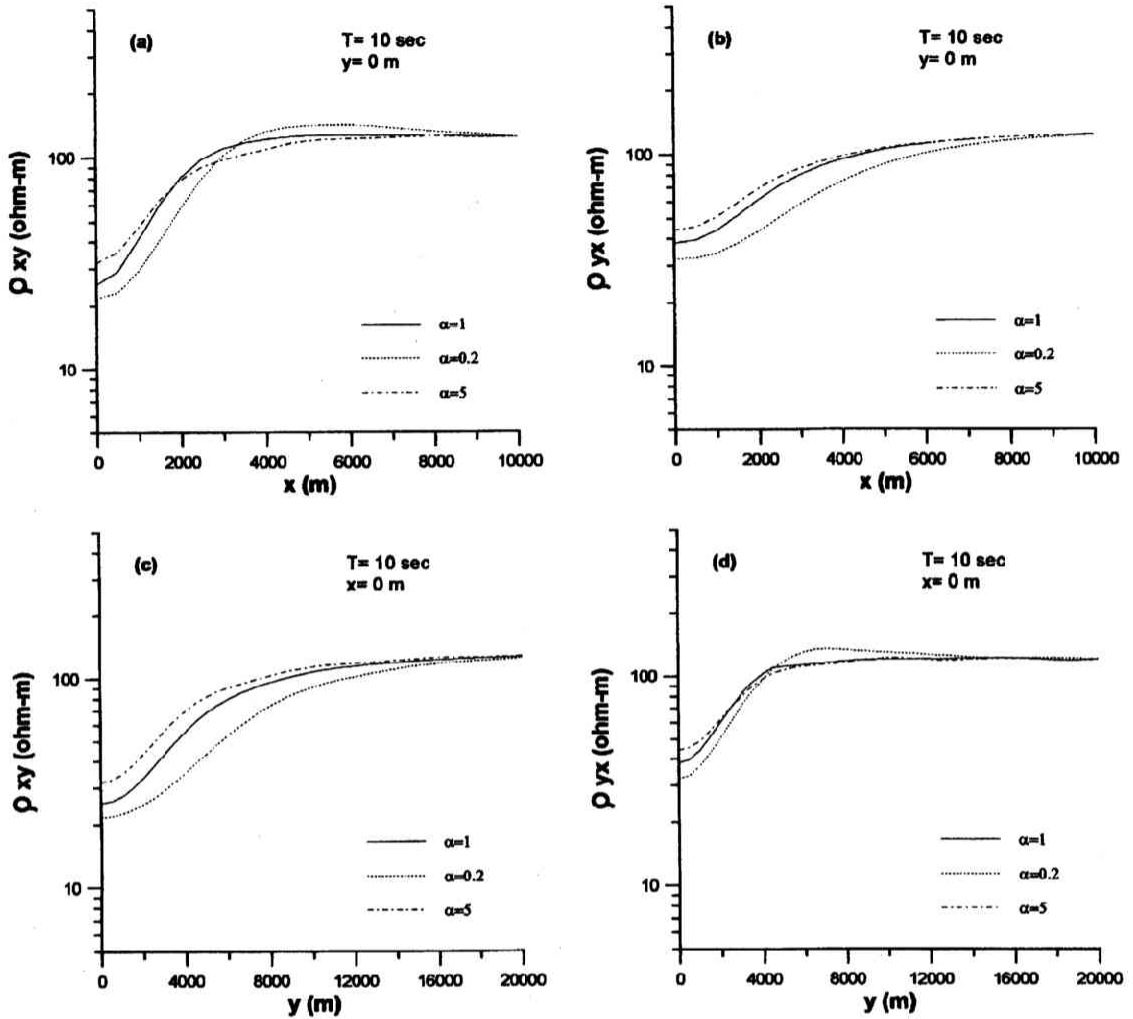


Fig. 10. Effect of sedimentary layer's vertical anisotropy on the apparent resistivity curves ρ_{xy} and ρ_{yx} .

greater or equal than one, but for completeness the other possibility was also considered.

Apparent resistivities and phases, calculated at $T = 10$ sec, are plotted in Figs. 10 and 11. The results obtained for each case show that the effects of the anisotropy are maxima at $x = y = 0$, and decrease as x or y increase, because then, vertical currents tend to disappear. It can be observed that, when $\alpha = 5$, apparent resistivities are greater and phases are lower than in the isotropic case, over the central zone of the basin. On the contrary, resistivities are lower and phases are greater than in the isotropic case, if $\alpha = 1/5$. We point out that these results were obtained just to show the effects exerted by the presence of an anisotropic layer in a concrete example, and not to make a general study of these effects. A discussion about this subject can be seen in Osella and Martinelli (1993), for the 2-D case.

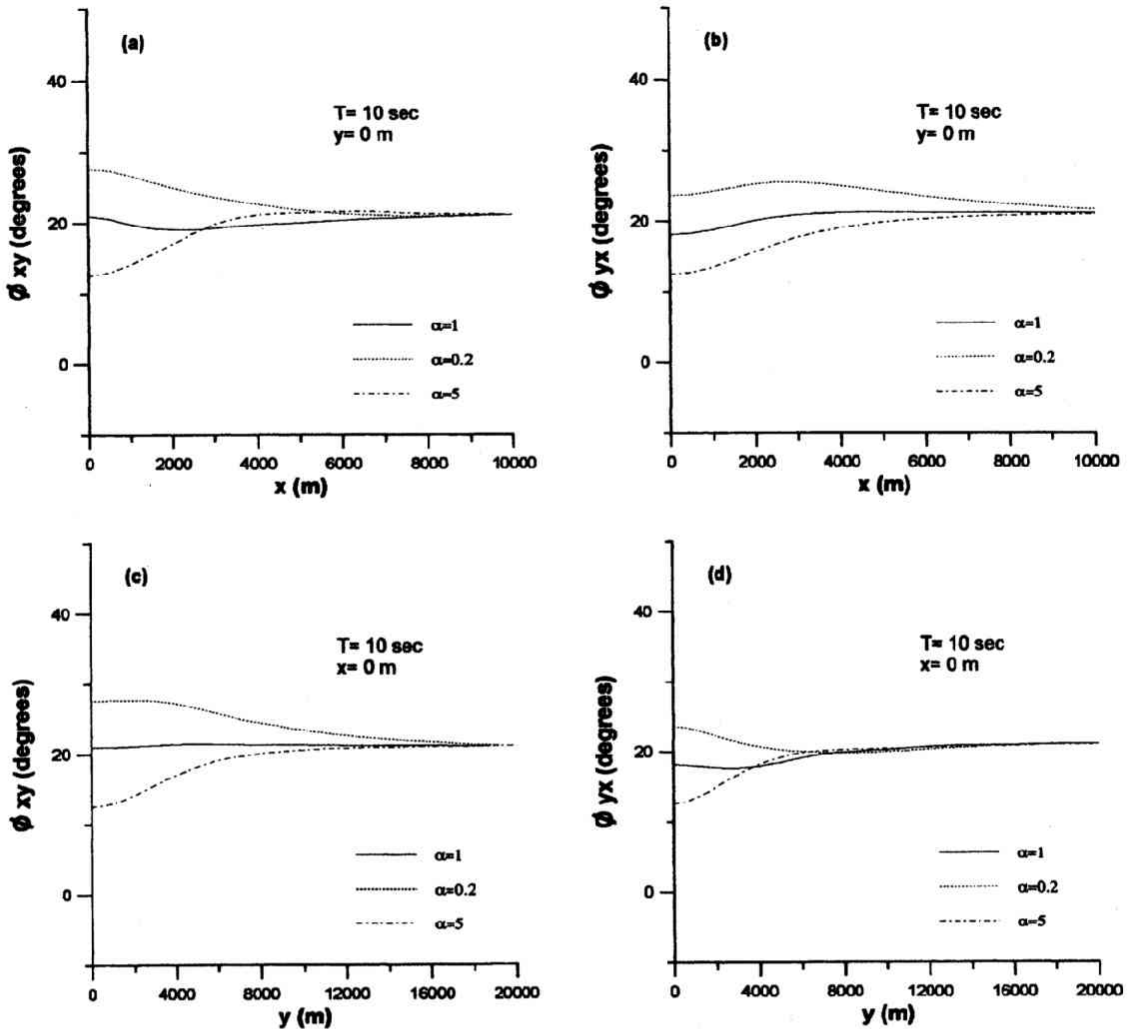


Fig. 11. The same as in Fig. 10 for the ϕ_{xy} and ϕ_{yx} curves.

5. Summary

Magnetotelluric data are usually interpreted applying 2-D methods. In many cases, reliable information can be obtained with this approach, but in others an adequate imaging of subsurface structure only can be achieved using 3-D techniques.

The increase of computational resources allowed the development of various 3-D methods during the last years.

In particular, IE methods can be used to model localized bodies intruded in layered media, while finite difference solutions permit the modeling of more general structures, assigning slowly varying conductivities to elements of three-dimensional grids.

In this paper, a method with a different applicability range is presented; it is intended for the modeling of multilayered structures with smooth irregular boundaries. In the formulation, the possibility of vertical anisotropy of the electrical conductivity of any layer, has also been included.

For all the methods mentioned above, memory requirements and processing times increase as the complexity of the structures does. For IE and FD techniques, the design of the grids becomes complicated; for RF method, the number of terms of the series that must be considered (defined by the value of the parameter L) and the number of points needed to calculate the integrals increase.

For the examples analyzed here, RF method showed good convergence. In the case of the conductive intrusion, similar processing times have been required for RF and IE modeling, a few minutes in a Sun Sparc station 20. For the anisotropic structures, the time has been larger, about 17 min for each period, due to the shape of the interface, which represented a more extended anomaly.

In the two cases considered, convergences were achieved taking $L = 10$, then 11 Mb of RAM memory were required, but 55 Mb were needed if L increased to 15.

This work was partially supported by CONICET, Universidad de Buenos Aires and Fundación Antorchas.

APPENDIX

For $l = m = 0$, Eqs. (30), (31) and (32) are given by:

$$\gamma_n^2 f_{00}^{(n)} - \frac{d^2 f_{00}^{(n)}}{dz^2} = 0, \quad (\text{A.1})$$

$$\gamma_n^2 g_{00}^{(n)} - \frac{d^2 g_{00}^{(n)}}{dz^2} = 0, \quad (\text{A.2})$$

$$h_{00}^{(n)} = 0. \quad (\text{A.3})$$

Then, the general solutions are:

$$\begin{aligned} f_{00}^{(n)}(z, \omega) &= (A_{00}^{(n)}(\omega) + C_{00}^{(n)}(\omega)) \exp(\gamma_n(\omega)z) \\ &\quad + (B_{00}^{(n)}(\omega) + D_{00}^{(n)}(\omega)) \exp(-\gamma_n(\omega)z), \end{aligned} \quad (\text{A.4})$$

$$\begin{aligned} g_{00}^{(n)}(z, \omega) &= (A_{00}^{(n)}(\omega) - C_{00}^{(n)}(\omega)) \exp(\gamma_n(\omega)z) \\ &\quad + (B_{00}^{(n)}(\omega) - D_{00}^{(n)}(\omega)) \exp(-\gamma_n(\omega)z), \end{aligned} \quad (\text{A.5})$$

$$h_{00}^{(n)}(z, \omega) = 0. \quad (\text{A.6})$$

When l or m are not 0, replacing Eq. (32) in Eqs. (30) and (31), it is obtained that:

$$(\alpha_n k_{ym}^2 + \gamma_n^2) f_{lm}^{(n)} - \frac{k_{ym}^2 + \gamma_n^2}{(R_{lm}^{(n)})^2} \frac{d^2 f_{lm}^{(n)}}{dz^2} - \alpha_n k_{xl} k_{ym} g_{lm}^{(n)} + \frac{k_{xl} k_{ym}}{(R_{lm}^{(n)})^2} \frac{d^2 g_{lm}^{(n)}}{dz^2} = 0, \quad (\text{A.7})$$

$$-\alpha_n k_{xl} k_{ym} f_{lm}^{(n)} + \frac{k_{xl} k_{ym}}{(R_{lm}^{(n)})^2} \frac{d^2 f_{lm}^{(n)}}{dz^2} + (\alpha_n k_{xl}^2 + \gamma_n^2) g_{lm}^{(n)} - \frac{k_{xl}^2 + \gamma_n^2}{(R_{lm}^{(n)})^2} \frac{d^2 g_{lm}^{(n)}}{dz^2} = 0. \quad (\text{A.8})$$

These equations can be uncoupled defining the functions $Is_{lm}^{(n)}$ and $An_{lm}^{(n)}$ in the form:

$$f_{lm}^{(n)} = \lambda k_{xl} Is_{lm}^{(n)} + \lambda k_{ym} An_{lm}^{(n)}, \quad (\text{A.9})$$

$$g_{lm}^{(n)} = \lambda k_{ym} Is_{lm}^{(n)} - \lambda k_{xl} An_{lm}^{(n)}. \quad (\text{A.10})$$

Then, replacing Eqs. (A.9) and (A.10) in Eqs. (A.7) and (A.8) and doing algebraic calculations, it can be proved that I_s and An satisfy:

$$\frac{d^2 I_{lm}^{(n)}}{dz^2} - (R_{lm}^{(n)})^2 I_{lm}^{(n)} = 0, \quad (\text{A.11})$$

$$\frac{d^2 An_{lm}^{(n)}}{dz^2} - (Q_{lm}^{(n)})^2 An_{lm}^{(n)} = 0. \quad (\text{A.12})$$

The solutions of these equations are given by:

$$I_{lm}^{(n)}(z, \omega) = A_{lm}^{(n)}(\omega) \exp(R_{lm}^{(n)}(\omega)z) + B_{lm}^{(n)}(\omega) \exp(-R_{lm}^{(n)}(\omega)z), \quad (\text{A.13})$$

$$An_{lm}^{(n)}(z, \omega) = C_{lm}^{(n)}(\omega) \exp(Q_{lm}^{(n)}(\omega)z) + D_{lm}^{(n)}(\omega) \exp(-Q_{lm}^{(n)}(\omega)z). \quad (\text{A.14})$$

So, from Eqs. (A.9) and (A.10):

$$f_{lm}^{(n)}(z, \omega) = \lambda k_{xl} (A_{lm}^{(n)}(\omega) \exp(R_{lm}^{(n)}(\omega)z) + B_{lm}^{(n)}(\omega) \exp(-R_{lm}^{(n)}(\omega)z)) \\ + \lambda k_{ym} (C_{lm}^{(n)}(\omega) \exp(Q_{lm}^{(n)}(\omega)z) + D_{lm}^{(n)}(\omega) \exp(-Q_{lm}^{(n)}(\omega)z)), \quad (\text{A.15})$$

$$g_{lm}^{(n)}(z, \omega) = \lambda k_{ym} (A_{lm}^{(n)}(\omega) \exp(R_{lm}^{(n)}(\omega)z) + B_{lm}^{(n)}(\omega) \exp(-R_{lm}^{(n)}(\omega)z)) \\ - \lambda k_{xl} (C_{lm}^{(n)}(\omega) \exp(Q_{lm}^{(n)}(\omega)z) + D_{lm}^{(n)}(\omega) \exp(-Q_{lm}^{(n)}(\omega)z)), \quad (\text{A.16})$$

and then, from Eq. (32):

$$h_{lm}^{(n)}(z, \omega) = \frac{\lambda k_{rlm}^2}{R_{lm}^{(n)}(\omega)} (A_{lm}^{(n)}(\omega) \exp(R_{lm}^{(n)}(\omega)z) - B_{lm}^{(n)}(\omega) \exp(-R_{lm}^{(n)}(\omega)z)). \quad (\text{A.17})$$

Finally, taking into account that $R_{00}^{(n)} = Q_{00}^{(n)} = \gamma_n$; Eqs. (A.4) to (A.6) and Eqs. (A.15) to (A.17) can be put in a general form valid for every l and $m \geq 0$:

$$f_{lm}^{(n)}(z, \omega) = (\lambda k_{xl} + \delta_{l0} \delta_{m0}) (A_{lm}^{(n)}(\omega) \exp(R_{lm}^{(n)}(\omega)z) + B_{lm}^{(n)}(\omega) \exp(-R_{lm}^{(n)}(\omega)z)) \\ + (\lambda k_{ym} + \delta_{l0} \delta_{m0}) (C_{lm}^{(n)}(\omega) \exp(Q_{lm}^{(n)}(\omega)z) \\ + D_{lm}^{(n)}(\omega) \exp(-Q_{lm}^{(n)}(\omega)z)), \quad (\text{A.18})$$

$$g_{lm}^{(n)}(z, \omega) = (\lambda k_{ym} + \delta_{l0} \delta_{m0}) (A_{lm}^{(n)}(\omega) \exp(R_{lm}^{(n)}(\omega)z) + B_{lm}^{(n)}(\omega) \exp(-R_{lm}^{(n)}(\omega)z)) \\ - (\lambda k_{xl} + \delta_{l0} \delta_{m0}) (C_{lm}^{(n)}(\omega) \exp(Q_{lm}^{(n)}(\omega)z) \\ + D_{lm}^{(n)}(\omega) \exp(-Q_{lm}^{(n)}(\omega)z)), \quad (\text{A.19})$$

$$h_{lm}^{(n)}(z, \omega) = \frac{\lambda k_{rlm}^2}{R_{lm}^{(n)}(\omega)} (A_{lm}^{(n)}(\omega) \exp(R_{lm}^{(n)}(\omega)z) - B_{lm}^{(n)}(\omega) \exp(-R_{lm}^{(n)}(\omega)z)). \quad (\text{A.20})$$

REFERENCES

- Bahr, K., Interpretation of the magnetotelluric impedance tensor: regional induction and local telluric distortion, *J. Geophys. Res.*, **62**, 119–127, 1988.
- Groom, R. and R. Bailey, Decomposition of magnetotelluric impedance tensors in the presence of local three-dimensional galvanic distortion, *J. Geophys. Res.*, **94**, 1913–1925, 1989.
- Hohmann, G. W., Three-dimensional induced polarization and electromagnetic modeling, *Geophys.*, **40**, 309–324, 1975.

- Jiracek, G. R., R. P. Reddig, and R. K. Kojima, Application of the Rayleigh-FFT technique to magnetotelluric modeling and correction, *Phys. Earth Planet. Inter.*, **53**, 365-375, 1989.
- Lippmann, B. A., Note on the theory of gratings, *J. Opt. Soc. Am.*, **43**, 408-414, 1953.
- Livelybrooks, D., Program 3-Dfeem: a multidimensional electromagnetic finite-element model, *Geophys. J. Inter.*, **114**, 443-458, 1993.
- Livelybrooks, D., M. Mareschal, E. Blais, and T. Smith, Magnetotelluric delineation of the Trillabelle massive sulfide body in Sudbury, Ontario, *Geophys.*, **61**, 971-986, 1996.
- Mackie, R., T. Madden, and P. Wannamaker, Three-dimensional magnetotelluric modeling using difference equations. Theory and comparisons to integral equation solutions, *Geophys.*, **58**, 215-226, 1993.
- Mackie, R., T. Madden, and S. Park, A three-dimensional magnetotelluric investigation of the California Basin and Range, *J. Geophys. Res.*, **101**, 16,221-16,239, 1996.
- Miller, R. F., On the Rayleigh assumption in scattering by a periodic surface, *Proc. Cambridge Phil. Soc.*, **69**, 217-225, 1971.
- Osella, A. and P. Martinelli, Magnetotelluric response of anisotropic 2-D structures, *Geophys. J. Inter.*, **115**, 819-828, 1993.
- Osella, A., C. Pomposiello, A. Favetto, C. Sainato, and P. Martinelli, Bidimensional modeling of a geothermal anomaly in the eastern border of Aconquija range, *Acta Geod. Geophys. Mont.*, **28**, 329-341, 1993.
- Pomposiello, C., A. Osella, A. Favetto, C. Sainato, P. Martinelli, and C. Aprea, Current channeling and 3-D effects detected from MT data at a sedimentary basin in Sierras Pampeanas, Argentina, *Geophys. J. Inter.*, 1996 (submitted).
- Smith, J. T. and J. Booker, Rapid inversion of two and three-dimensional magnetotelluric data, *J. Geophys. Res.*, **96**, 3905-3922, 1991.
- Wannamaker, P., Advances in three-dimensional magnetotelluric modeling using integral equations, *Geophys.*, **11**, 1716-1728, 1991.
- Wannamaker, P., J. Stodt, and L. Rijo, A stable finite element solution for two-dimensional magnetotelluric modeling, *Geophys. J. R. astr. Soc.*, **88**, 277-296, 1987.